ANALYSIS OF REACTOR MATERIAL EXPERIMENTS INVESTIGATING CORIUM CRUST STABILITY AND HEAT TRANSFER IN JET IMPINGEMENT FLOW

CONF-850810--9

DE85 007980

by

J. J. Sienicki and B. W. Spencer

Reactor Analysis and Safety Division
Argonne National Laboratory
Argonne, Illinois 60439

INTRODUCTION

An important issue in the assessment of hypothetical severe accident sequences in light water reactors is the rate of downward migration of the core melt materials following the inception of core degradation. As downward motion progresses, the corium will eventually drain onto support structures such as the core support plate, various coolant flow distribution plates, and ultimately the reactor pressure vessel lower head. The corium freezing and/or steel ablation behavior which results when the molten corium contacts the relatively cold structural members plays a role in determining the timescale of the downward progression and may additionally play a role in determining the manner in which the lower head fails. A principal mode of interaction between corium and structure involves the impingement of a molten corium stream normally upon the structure. A fundamental issue in the basic mechanisms underlying corium-structure interactions is the presence or absence of a solidified layer, or crust, of corium interstitial to the flowing molten corium and the structure substrate, tending to insulate the structure from the hot molten corium (Figure 1). Crust formation in impingement flow was studied previously by Epstein et al. (1) using simulant material experiments in which a freezing liquid was impinged upon the end of a meltable rod. The simulant tests exhibited ablation rates consistent with the existence of a protective crust.

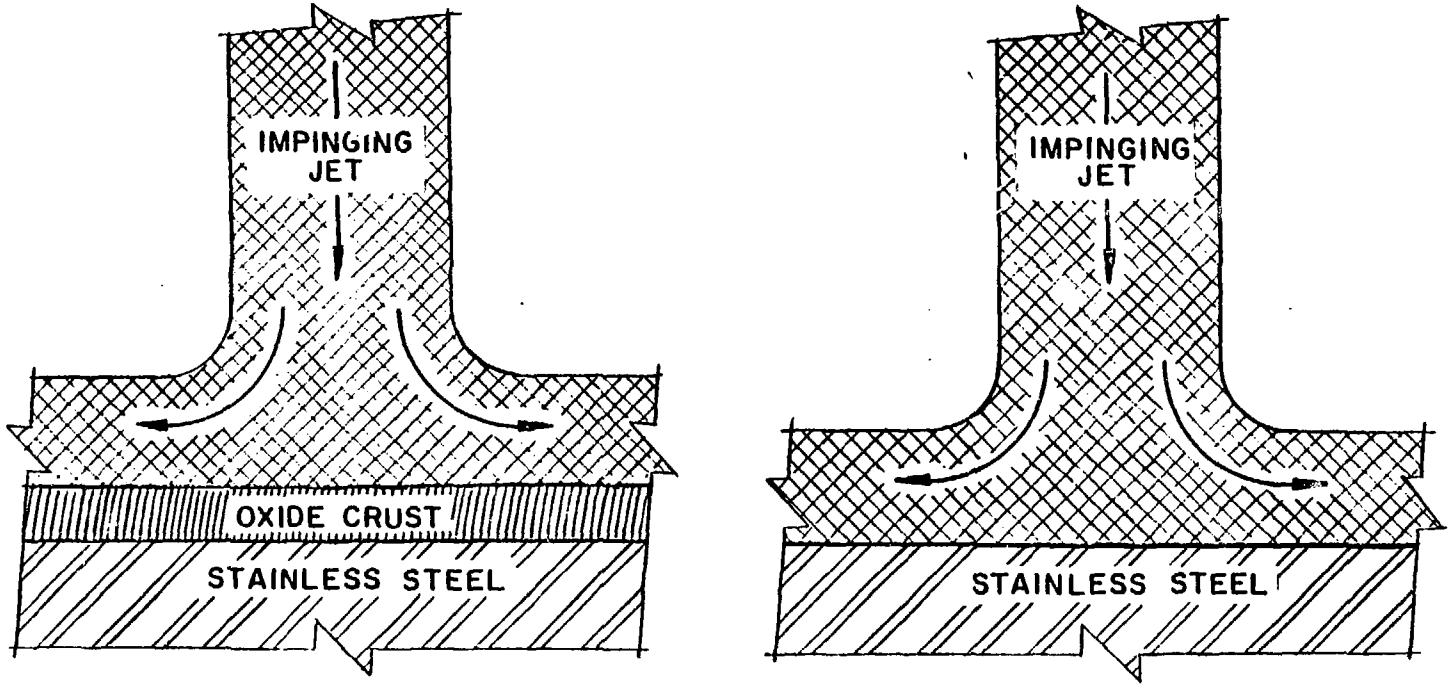

Figure 1. Illustration of Impingement of Molten Corium Jet onto Solid Stainless Steel Plate with and without Formation of Stable Crust of Solidified Corium upon Steel Substrate.

Presented here is an analysis of the results of the CSTI-1, CSTI-3, and CWTI-11 reactor material experiments in which a jet of molten corium initially at 3080 K was directed downward upon a stainless steel plate. The experiments are a continuation of a program of reactor material tests (2 to 4) investigating LWR severe accident phenomena. The objective of the present analysis is to determine the existence or nonexistence of a corium crust during impingement from comparison of the measured heatup of the plate (as measured by thermocouples imbedded immediately beneath the steel surface) with model calculations assuming alternately the presence and absence of a stable crust during impingement.

SUMMARY OF EXPERIMENTS

The corium mixture employed in the experiments consisted of 60% UO_2, 16% ZrO_2, and 24% stainless steel generated by a thermite reaction at an initial temperature of 3080 K, approximately 160 K above the liquidus temperature of the oxide phase (2923 K). Conditions for the three tests are given in Table 1. Figure 2 shows the apparatus used for the two Corium-Structure Thermal Interaction (CSTI) Tests, CSTI-1 and CSTI-3. The thermite reaction was carried out within a thick-walled stainless steel thermite vessel. Following the completion of the reaction, the corium was released by the actuation of a fast acting slide mechanism in CSTI-1 and meltthrough of a thin stainless steel diaphragm in CSTI-3. The corium mixture flowed through a 2.54 cm diameter injection opening. The stainless steel (Type 304) plate upon which the corium impinged was 1.27 cm thick, 21.2 cm in diameter, and was supported by a similar 3.81 cm thick base plate. The distance from the bottom of the injection opening to the plate was 35 cm; the centerlines were carefully aligned so that the impinging jet would be centered on the plate. In CSTI-1 and CSTI-3, the plate was contained within a cylindrical interaction vessel which confined

TABLE 1. CONDITIONS OF CORIUM JET IMPINGEMENT TESTS

Test	CSTI-1	CSTI-3	CWTI-11
Injection Opening Diameter, cm	2.54	2.54	2.54
Height of Injection Opening above Plate, cm	34.9	34.9	35.2
Initial Plate Temperature, K	299	299	385
Mass of Reactants Loaded, kg	4.10	4.10	4.10
Mass of Fuel Injected, kg	2.43	3.30	2.93
Thermite Vessel Pressure at Onset of Injection, MPa	0.118	0.55	5.09
Impingement Duration, s	~ 0.5	~ 0.1	~ 0.12

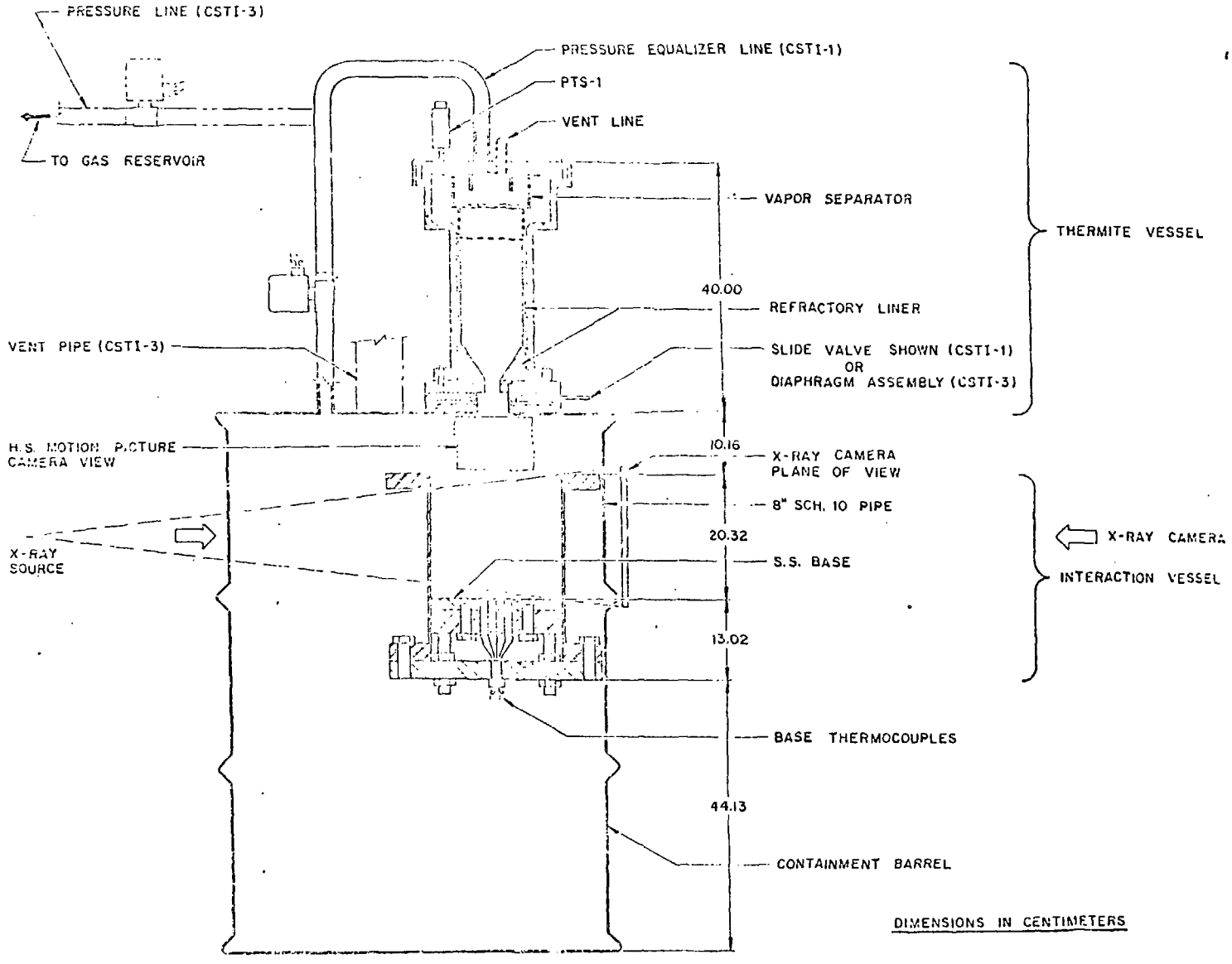

Figure 2. Illustration of Apparatus Used in Corium-Structure Thermal Interaction Tests CSTI-1 and CSTI-3.

the corium following impingement tending to form a pool of corium atop the plate. The interaction vessel was open at the top to avoid any significant pressurization and was surrounded by a filtered-vented steel drum to retain any corium which might splash out of the vessel.

The CWTI-11 experiment was carried out in the ANL/EPRI COREXIT Facility (2, 3). Although the principal objective of the test was to investigate the direct heating of the containment atmosphere associated with the gas-driven sweepout of corium, an instrumented stainless steel plate was used for the base of the interaction vessel to obtain additional data on impingement flow heat transfer. In this test, the interaction vessel was not open at the top. Instead, the injected corium was free to flow laterally from the closed vessel through a 10.8 cm diameter elbow-shaped pipeway and enter a large expansion volume. The corium injection was followed by a high velocity follow-on gas flow which tended to levitate remaining molten corium in a dispersed droplet flow regime inside the interaction vessel resulting in freezing out of corium upon the vessel walls and top cover as well as sweepout of corium out of the interaction vessel through the pipeway. The follow-on gas flow thereby limited the amount of corium accumulated atop the plate following the impingement phase. In posttest examination, a corium mass of 0.699 kg was recovered from atop the plate compared with an injected mass of 2.93 kg; the remainder had undergone sweepout or had frozen out upon the interaction vessel walls and cover.

The velocity and flow regime of the impinging corium jet were varied among the three tests. In CSTI-1, corium was near gravity dropped onto the plate. In CSTI-3 and CWTI-11, the injections were pressure driven at initial driving pressure drops of 0.45 and 4.99 MPa respectively; the high injection pressure achieved in CWTI-11 is believed to have given rise to a two-phase

flow regime involving the injection of significant gas together with the corium.

The principal data recorded during the experiments was the response of ten thermocouples (TC's) imbedded into the steel plate from the underside. The TC locations and depths are shown in Figure 3 for CSTI-3 and CWTI-11. The locations were selected to provide heatup data at various radial locations encompassing the jet stagnation region. Additional information was obtained from posttest examination of the corium debris and the plate.

After the corium debris was removed, no major melting of the steel plate was observed. However, there were areas where some minor pitting of the surface had occurred. The pitting was very localized and isolated. In CSTI-1, pitting was located between 2.5 and 6.3 cm from the jet axis. The largest pocket of erosion measured ~ 2 cm diameter, 3 mm maximum depth, and was centered at 3.8 cm from the axis. In CSTI-3, pitting was limited to two regions of ~ 2 cm equivalent diameter, 2 mm maximum depth, which were centered at ~ 1.0 and 3.2 cm from the plate centerline. The melted steel in CSTI-3 appeared to have been effectively swept out of the pitted zones by the jet. The edges of the pits were sharp and deepest nearest the center, further indicating a remarkably abrupt spatial variation in the surface attack. The pitting in CWTI-11 occurred in an annular region at a mean radius of ~ 3 cm from the axis. The annulus radial thickness varied circumferentially ranging between zero and a maximum of ~ 2 cm.

CALCULATIONAL MODEL

To interpret the measured TC temperatures and assess their implications for stable crust formation, a computer model was developed to predict the heatup of the TC's when corium is injected atop a planar surface. Both of the cases in which a stable crust is assumed to be either present or absent during the impingement phase (Figure 1) are modeled.

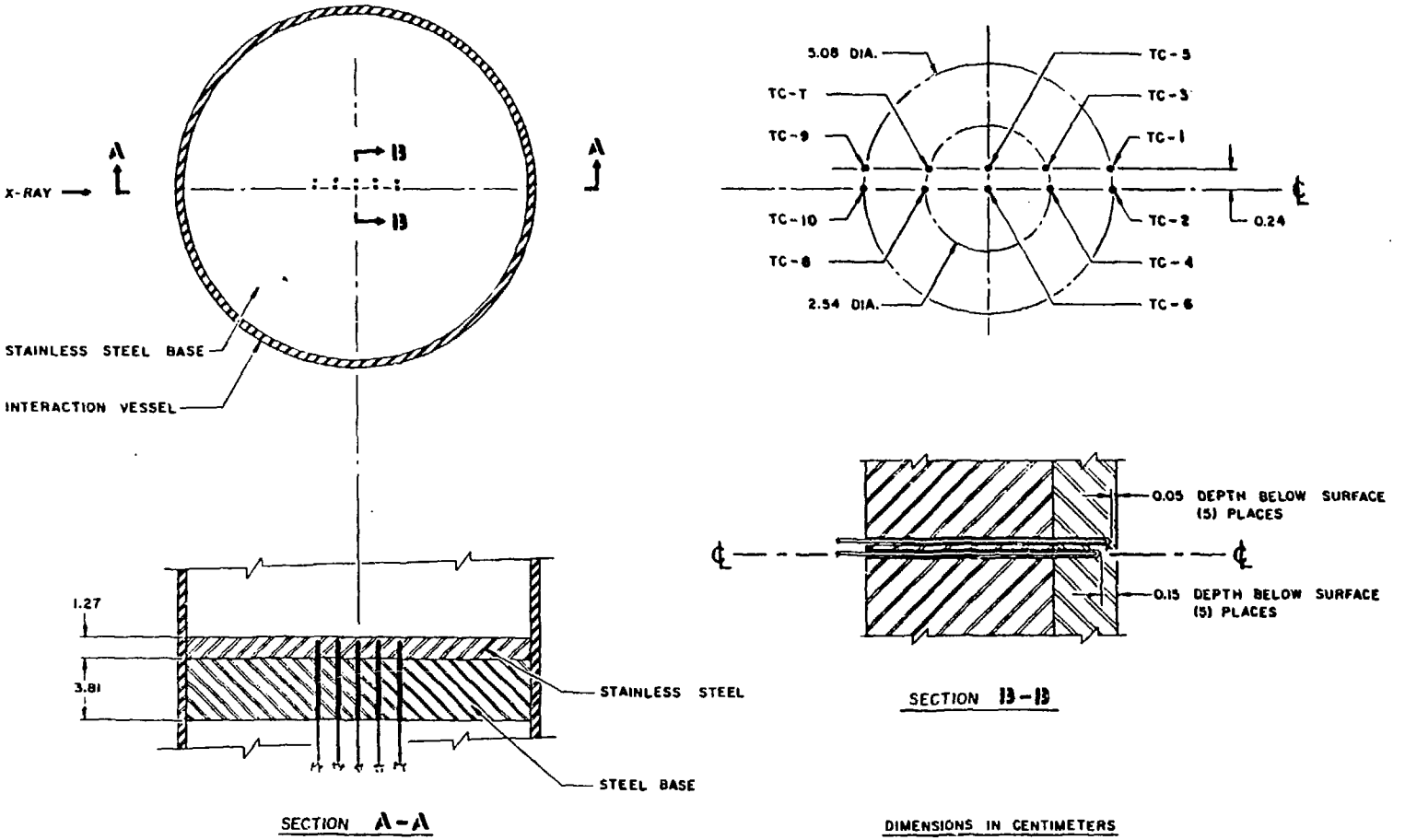

Figure 3. Location of Thermocouples in Stainless Steel Plate for CSTI-3 and CWTI-11.

When stable crust formation is assumed during the impingement phase, the model calculates the growth of the crust layer consistent with forced convection heat transfer from the impinging molten corium and thermal conduction downward through the crust and plate. Specifically, the local thickness of the crust satisfies the equation,

$$\rho_f L_f \frac{d\delta}{dt} = k \frac{\partial T}{\partial z} - h_{conv} (T_f - T_{f,freeze}). \quad (1)$$

The thermal gradient is evaluated within the crust at its upper surface. The heat transfer coefficient, h_{conv}, accounts for the effects of forced convection from the flowing corium to the crust. The downward heat flux from the flowing melt to the solid crust layer is proportional to the difference between the impinging molten corium temperature, T_f, and the temperature at the crust upper surface which is equal to the corium freezing temperature, $T_{f,freeze}$. For the experiments, this temperature difference has a value of $\sim$ 160 K. Heat transfer coefficients describing forced convection heat transfer in jet impingement flow are generally dependent upon the radial distance from the centerline. In the model, the radial dependency of the plate heatup arising from that of the heat transfer coefficient is accommodated by dividing the plate into successive radial zones corresponding to

$$\frac{r}{D} < 0.5, \quad 0.5 \leq \frac{r}{D} < 1.0, \quad 1.0 \leq \frac{r}{D} < 2.0, \quad \text{etc.},$$

where D is the impinging jet diameter. The heat transfer coefficient is assumed constant within each of these regions and is defined such that the heat transfer coefficient averaged over each of the discs equals the maximum values recommended by Martin (5) for circular jet impingement heat transfer.

To facilitate computation, the following fits were made to the recommended disc averaged Nussett numbers presented graphically in Reference 5:

$$Nu = 1.02\ Re^{0.513} Pr^{0.42}, \quad \text{for } \frac{r}{D} < 0.5\ ; \tag{2a}$$

$$Nu = 0.606\ Re^{0.547} Pr^{0.42}, \quad \text{for } \frac{r}{D} < 1.0\ ; \tag{2b}$$

$$Nu = 0.336\ Re^{0.584} Pr^{0.42}, \quad \text{for } \frac{r}{D} < 2.0\ . \tag{2c}$$

Values of the resulting convective heat transfer coefficients, h_{conv}, calculated for each of the radial regions are shown in Table 2 for the experiments. In evaluating the coefficients, the jet diameter has been taken equal to that of the injection opening. The radial variation of the heat transfer coefficient is observed to be only moderate; h_{conv} decreases by no more than 28% in going from the central to the outermost of the regions considered here.

A one-dimensional calculation of the heatup of the plate is performed within each radial zone. Azimuthal symmetry is assumed and radial heat transfer between crust or steel in neighboring radial regions is not modeled. Inside each radial zone, an axial mesh is defined upon the corium region above the plate, the plate itself, and the underlying base plate. Crust growth is calculated by either of two methodologies depending upon the instantaneous crust thickness. The one-dimensional calculation of the dynamics of "thin" crusts having a thickness less than that of the bottommost corium mesh cell employs the refined integral heat balance method of Volkov and Li-Orlov (6) to account for the effects of the temperature profile within the crust. Thicker crusts are described with a one-dimensional, multicell finite difference calculation coupled to a continuous tracking of the flowing melt/crust interface

TABLE 2. VALUES OF FORCED CONVECTION HEAT TRANSFER COEFFICIENT ASSUMED FOR CORIUM JET IMPINGEMENT FLOW

Test	$h(\frac{r}{D} < 0.5)$, $W/(m^2 \cdot K)$	$h(0.5 \leq \frac{r}{D} < 1.0)$, $W/(m^2 \cdot K)$	$h(1.0 \leq \frac{r}{D} < 2.0)$, $W/(m^2 \cdot K)$
CSTI-1	470	405	340
CSTI-3 (Onset of Impingement)	870	815	731
CSTI-3 (End of Impingement)	841	786	703
CWTI-11	752	694	616

as it moves vertically across the corium mesh cells in each radial region. The calculation of the heatup of the stainless steel plate employs the refined integral heat balance approach until the thermal boundary layer reaches the center of the topmost plate mesh cell and then switches to a multicell, finite difference calculation. Following the completion of corium impingement, the solidification of the molten corium pool accumulated atop the crust and the continued heatup of the plate is predicted by continuing the finite difference calculations which are then extended to also encompass the molten pool. The corium and stainless steel structure are described with temperature dependent thermophysical properties. The code models the corium as a heterogeneous mixture in which the metallic phase is dispersed as fine droplets throughout an oxide continuum. In the calculations, the corium is assumed to freeze at a single temperature equal to the liquidus temperature of the oxide phase (2923 K).

In the absence of crust formation, the calculation during the impingement phase is identical to that which would describe the impingement of a non-freezing jet. Specifically, heat is assumed to be transferred by forced convection directly from the flowing melt to the plate. The downward heat flux from the impinging corium is thus equal to h_{conv} $(T_f - T_{s,i})$ where $T_{s,i}$ is the temperature at the corium/steel interface at the plate upper surface. The downward heat flux from the impinging jet is proportional to the difference between the molten corium temperature and the plate surface temperature. The temperature differences in this case may be significantly greater than those with a crust. For example, if the stainless steel is heated to its melting temperature (~ 1700 K), the driving temperature difference has a value of 1280 K. It follows that significant differences in the plate heatup rate may be expected between calculations assuming the presence and absence of a stable

crust. If steel melting is predicted by the code, the molten steel is assumed to remain stationary above the solid steel substrate; the effects of flow of molten steel as a film or physical removal of molten steel are not treated in the present calculations. The heatup of the steel in each radial region is calculated with a one-dimensional finite difference calculation as described above. Following the corium impingement phase, the thermal equilibration of the stationary corium pool accumulated upon the plate with the stainless steel is calculated with a finite difference analysis as in the case where a crust is always present. It should be noted that pool solidification takes place with the growth of a frozen corium layer atop the plate and a solid/liquid interface which moves upward through the pool. The frozen corium layer in this case is also a crust. The point here is that the calculations "without crust" model a situation in which it is postulated that phenomena associated with corium flow and jet impingement (eg., turbulence) somehow prevent the formation of a thin insulating layer of solid corium interstitial to the flowing hot corium and the plate during the preceding impingement phase.

A significant part of the analysis is the calculation of the TC temperature from the surrounding plate temperature. As shown in Figure 4, the diameter of the TC's (1.49 mm) is slightly less than that of the holes into which they are seated (1.65 mm) and the TC hemispherical head does not conform to the pointed contour of the hole. Consequently, the thermal resistance associated with conduction across the air gap separating the TC from the surrounding plate steel causes the TC temperature to lag behind the temperature of the plate. The TC's are of the grounded junction type in which the junction has the form of a bead on the inner surface of the sheath. The code predicts the junction temperature by treating the junction and sheath material comprising the hemispherical head as a bulk medium and accounting for the thermal

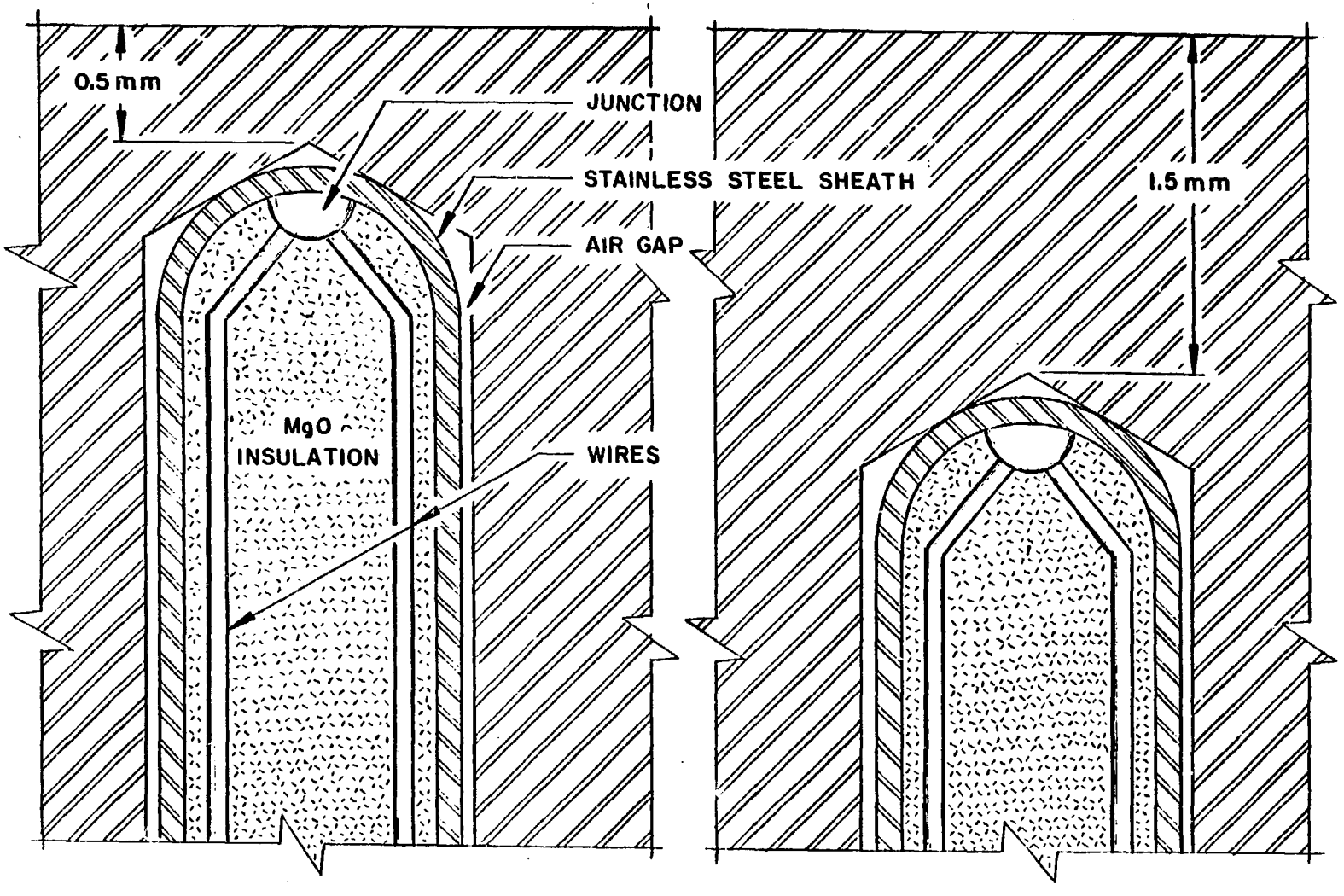

Figure 4. Illustration of Placement of Thermocouples inside Holes Drilled into Stainless Steel Plate from Underside in CSTI-3 and CWTI-II.

resistance of the air gap as well as the heat loss into the underlying TC MgO insulation.

RESULTS

In general, the calculations predict that if a stable crust is present throughout the impingement phase, then melting of the steel plate should not occur. On the other hand, the complete absence of a crust during impingement results in the calculation of steel melting near the surface. The only evidence of steel melting observed in posttest examination of the plate was the localized and isolated pitting which encompassed only a small fraction of the plate total surface area. Thus, the lack of melting over nearly all of the plate surface is consistent with the existence of a corium crust during the impingement phase.

For those TC's which are not located in a region where pitting occurred, the measured TC temperatures during and immediately following corium impingement are either in good agreement with or are bounded by the model predictions assuming an invariably stable crust is present as corium impinges upon the plate. For CSTI-3, Figure 5 compares the measured and calculated temperatures for those TC's located at a radius of 2.54 cm from the centerline and a depth of 0.5 mm. Similarly, Figure 6 shows the comparison for the other TC's at this radius but imbedded 1.5 mm beneath the surface. Temperatures are shown for the first 1 s of time following the onset of impingement (compared with an injection timescale of ~ 0.1 s). Longer time intervals are not considered here, because as the timescale is increased, the heat input to the plate during the impingement phase represents a relatively lower portion of the total cumulative heat input which also includes that removed from the pool formed atop the crust or plate. The recorded temperatures agree well with those predicted assuming the presence of a crust throughout the impingement process.

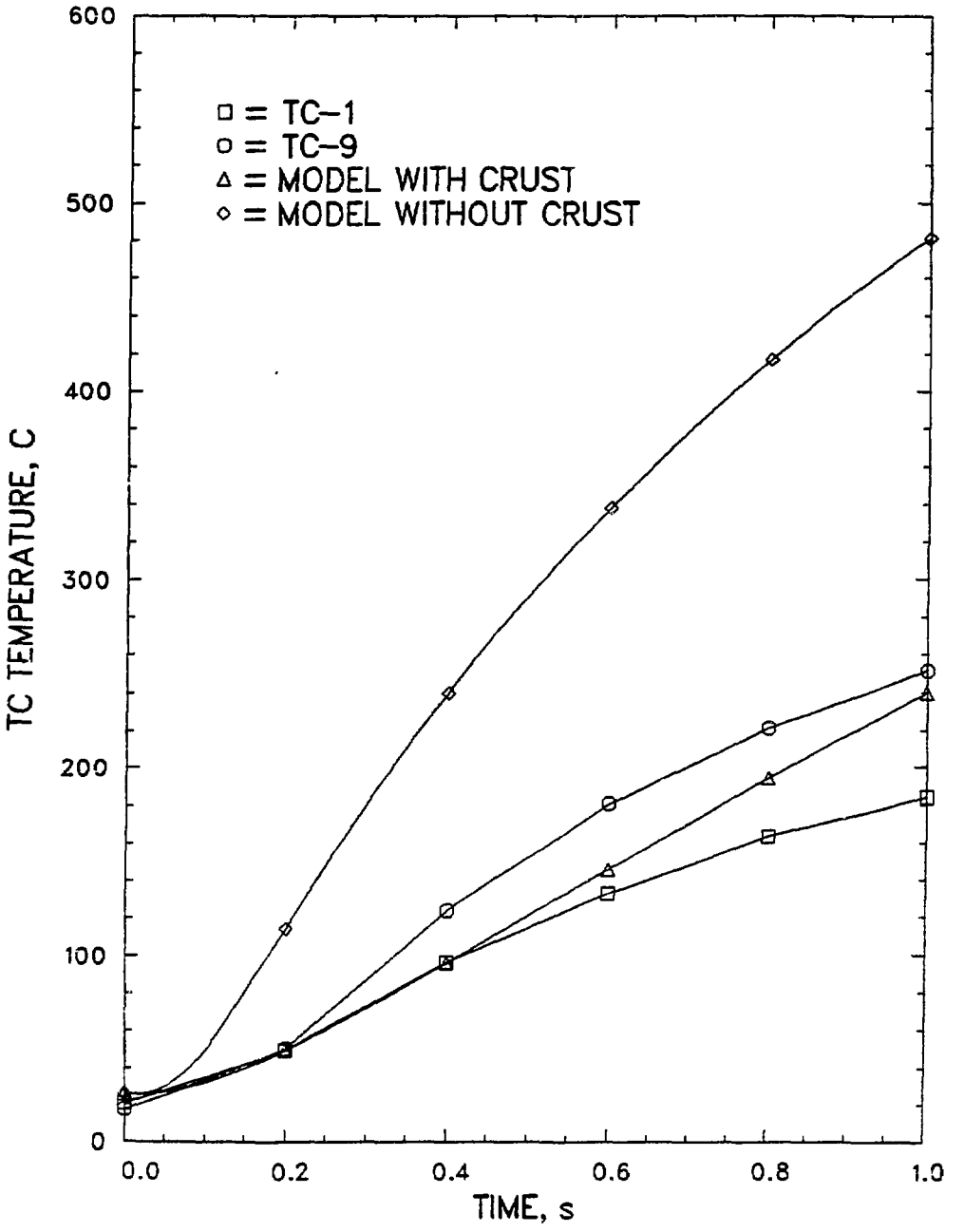

Figure 5. Comparison of Measured and Predicted Thermocouple Temperatures for CSTI-3: Thermocouples 2.54 cm from Centerline and 0.5 mm below Surface.

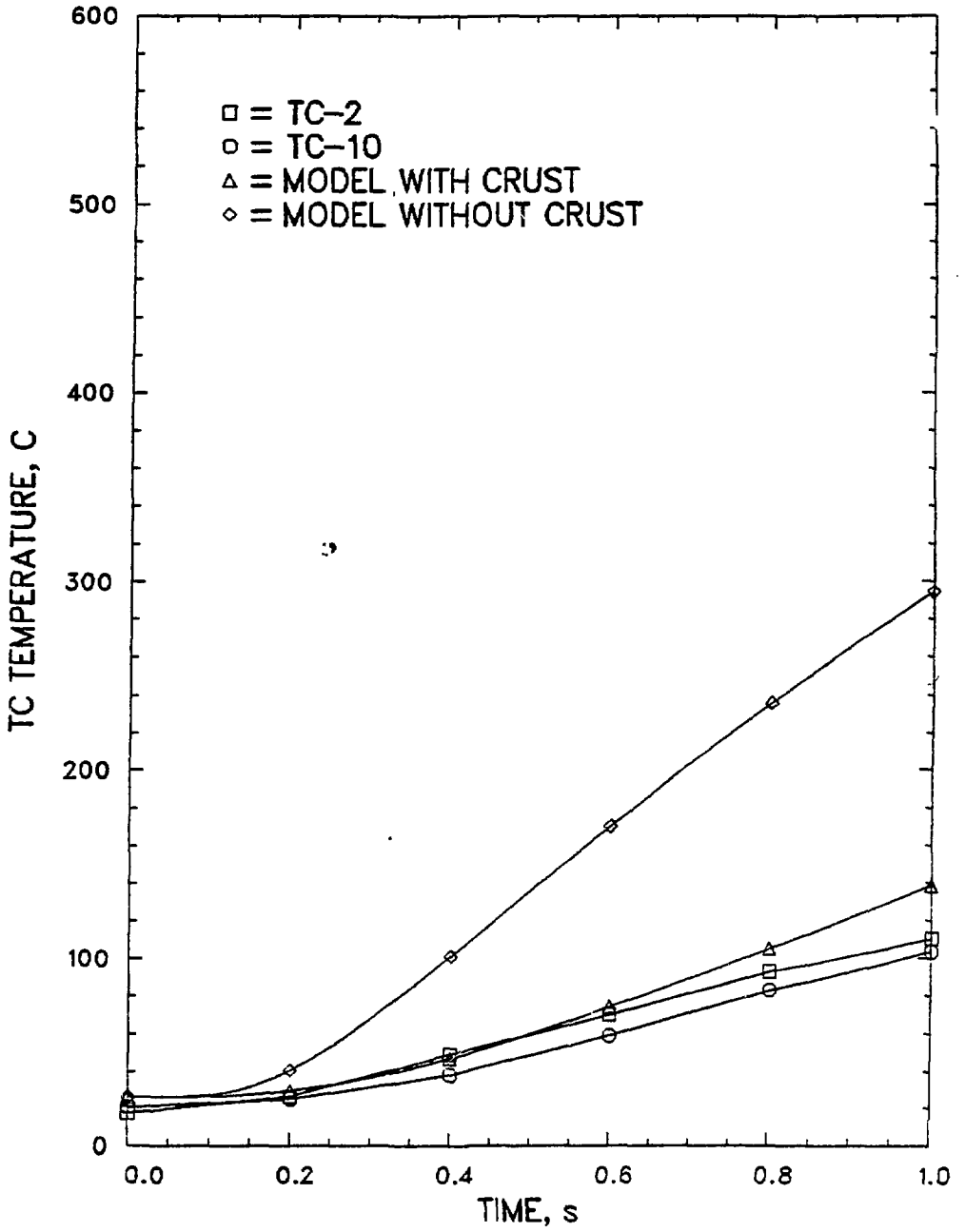

Figure 6. Comparison of Measured and Predicted Thermocouple Temperatures for CSTI-3: Thermocouples 2.54 cm from Centerline and 1.5 mm below Surface.

In contrast, the temperature rise over the first second calculated assuming the absence of a crust is more than twice as large as that predicted with a crust. This indicates that the short time thermal response of the plate is a viable probe of the insulating effects of crust formation. It should also be noted that the temperatures measured on opposite sides of the centerline (i.e., TC-1 vs. TC-9) may show considerable variation among themselves (but much less than the crust/no crust difference) suggesting some angular variation to the heat transfer phenomena in the experiments.

A significantly different behavior is obtained for TC's underlying a surface which has undergone pitting. Figures 7 and 8 show the comparison between calculation and experiment for those TC's at a radius of 1.27 cm from the jet axis. Pitting did not occur above TC-3 or TC-4 and the temperatures measured at these locations agree with the calculations assuming an invariably stable crust. Fortuitously, TC-7 and TC-8 were situated in one of the two isolated regions where pitting had taken place. The temperature measured by TC-7 for the first ~ 0.6 s is observed to agree well with that predicted assuming that crust formation is nonexistent. The initial temperature rise rate for TC-8 also corresponds more to that calculated in the absence of a crust and the temperature at 1 s lies midway between the predictions with and without a crust. In contrast to all other TC data as well as the model calculations, TC-5 (Figure 9) exhibited a very rapid rise of 440 K over 0.09 s and 520 K by 0.2 s. The peak temperature of 812 K is comparable to the theoretical interface temperature (7) achieved immediately following the sudden and perfect contact of semi-infinite slabs of corium and stainless steel (825 K) suggesting that the rapid temperature rise may reflect the removal of steel overlying the TC and essentially direct contact of the TC with hot corium. Upon examination of the plate, it was observed that the initial 0.5 mm thickness of steel

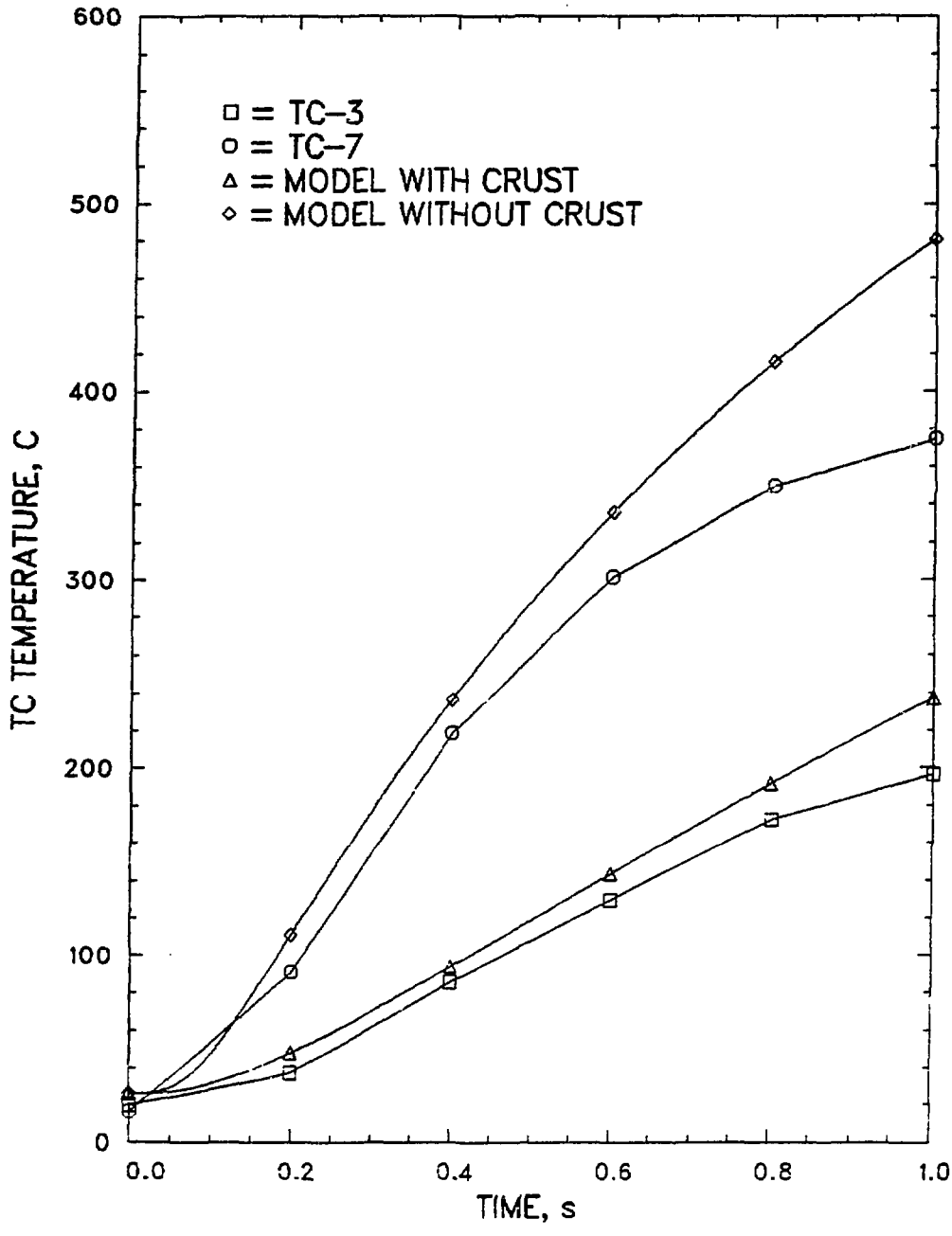

Figure 7. Comparison of Measured and Predicted Thermocouple Temperatures for CSTI-3: Thermocouples 1.27 cm from Centerline and 0.5 mm below Surface.

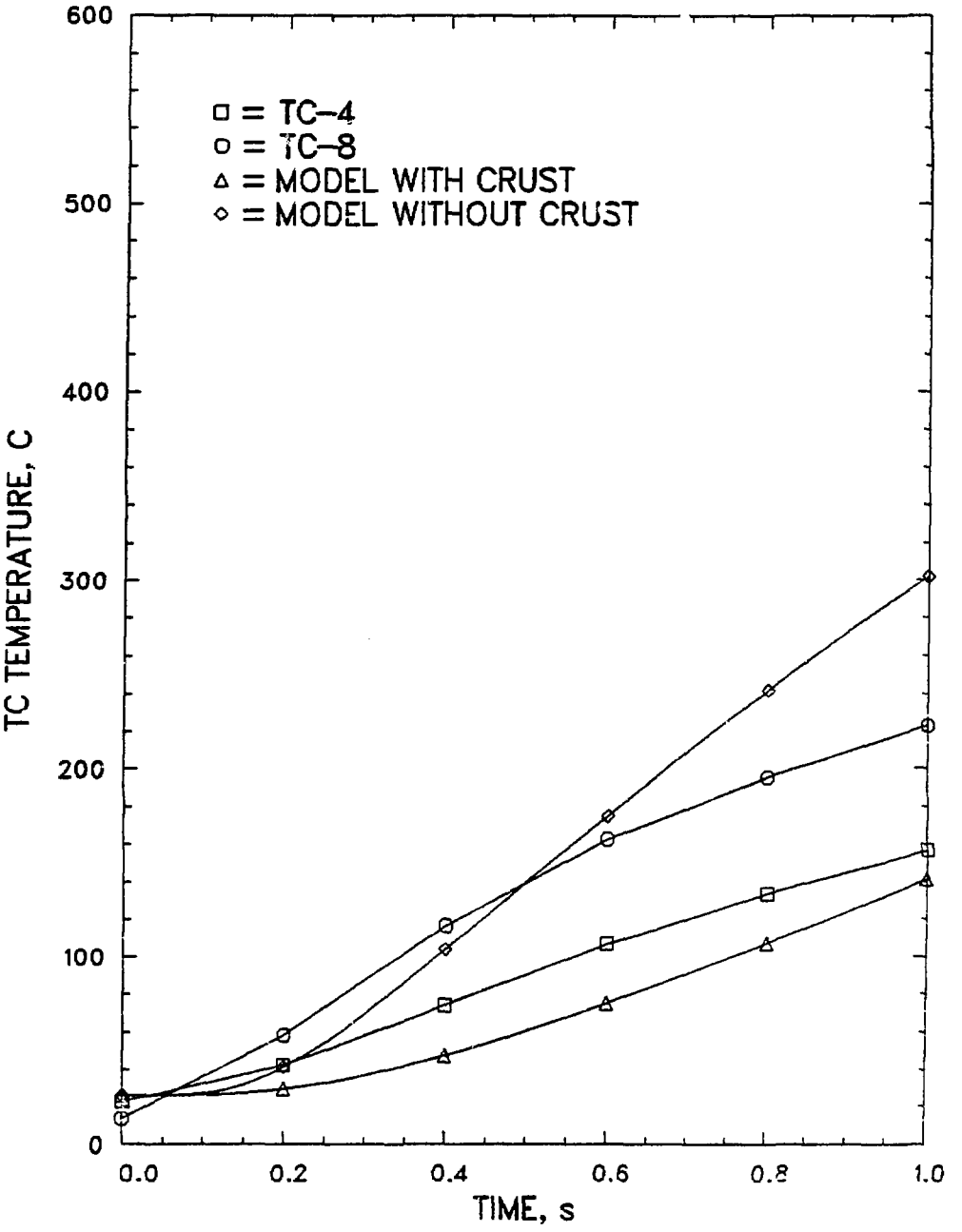

Figure 8. Comparison of Measured and Predicted Thermocouple Temperatures for CSTI-3: Thermocouples 1.27 cm from Centerline and 1.5 mm below Surface.

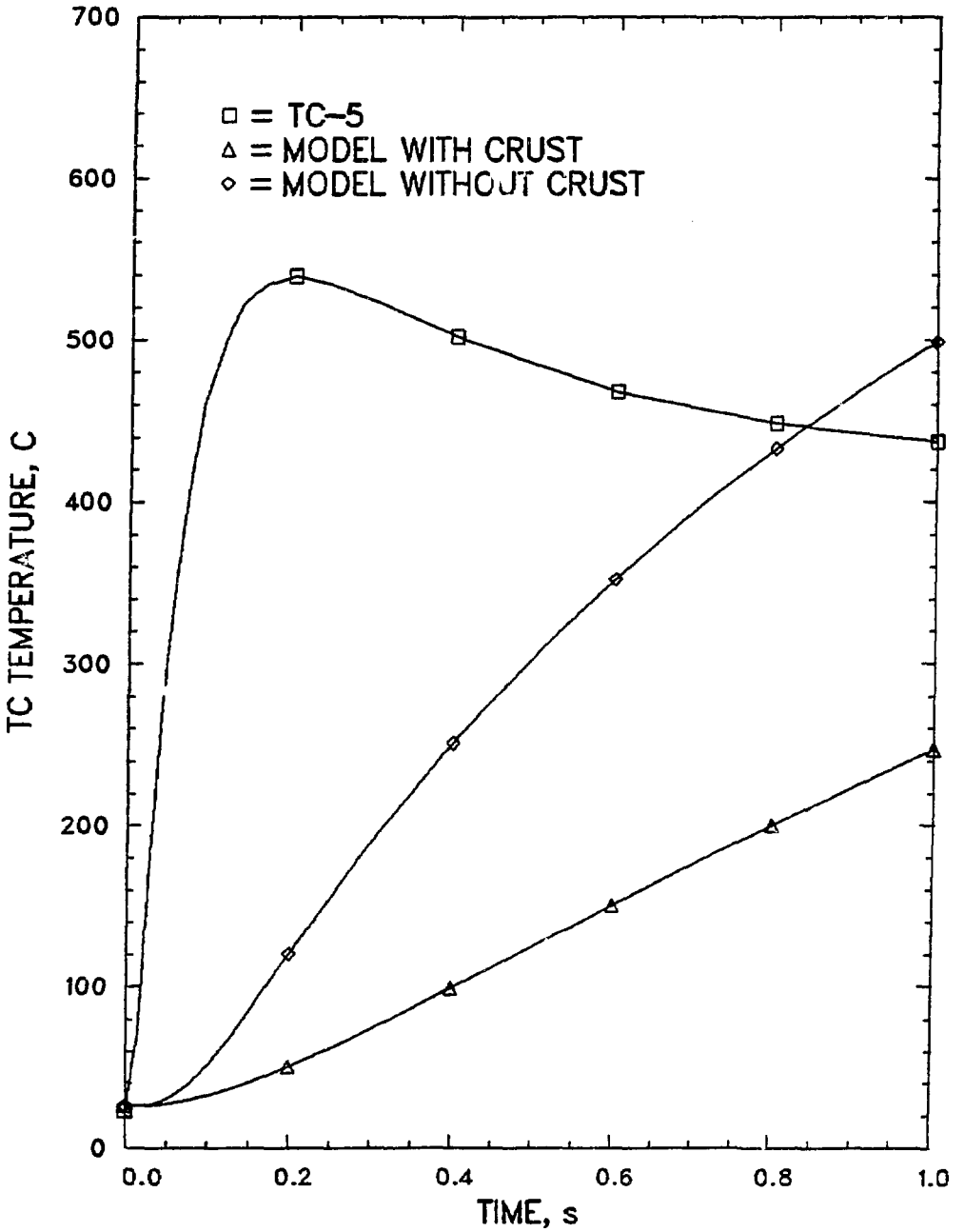

Figure 9. Comparison of Measured and Predicted Thermocouple Temperatures for CSTI-3: Thermocouple 0.24 cm from Centerline and 0.5 mm below Surface.

above TC-5 and TC-7 had been eroded away (i.e., the holes into which the TC's fit were completely "burned through").

For CWTI-11, the recorded TC temperatures agree most closely with those predicted assuming that a stable crust is present throughout the impingement phase (Figures 10-15). The major discrepancy between calculation and experiment was obtained for TC-5 for which the measured temperature lies significantly below that calculated with a crust. In CSTI-1, the depths of the TC's beneath the surface (2, 4, and 8 mm) significantly exceeded those subsequently employed in CSTI-3 and CWTI-11 resulting in a reduced sensitivity of the measured TC heatup to the existence of a crust for CSTI-1. Although results from a detailed comparison for CSTI-1 shall not be shown here, the measured TC responses in that experiment are all consistent with predictions assuming protective crust formation.

CONCLUSIONS

Comparison of the measured thermocouple temperatures with model calculations indicates that a protective crust of solidified corium was present over nearly all of the plate surface area throughout the impingement process. The calculations also show that the crust tended to significantly insulate the plate from the flowing hot molten corium, reducing the initial thermocouple heatup rate by more than a factor of two below that calculated in the absence of crust formation. Although a crust was present over nearly all of the plate surface, the experiments also show evidence for very localized and isolated crust removal and steel melting as revealed by the localized and isolated pitting of the steel surface and the response of thermocouples located within the pitted region.

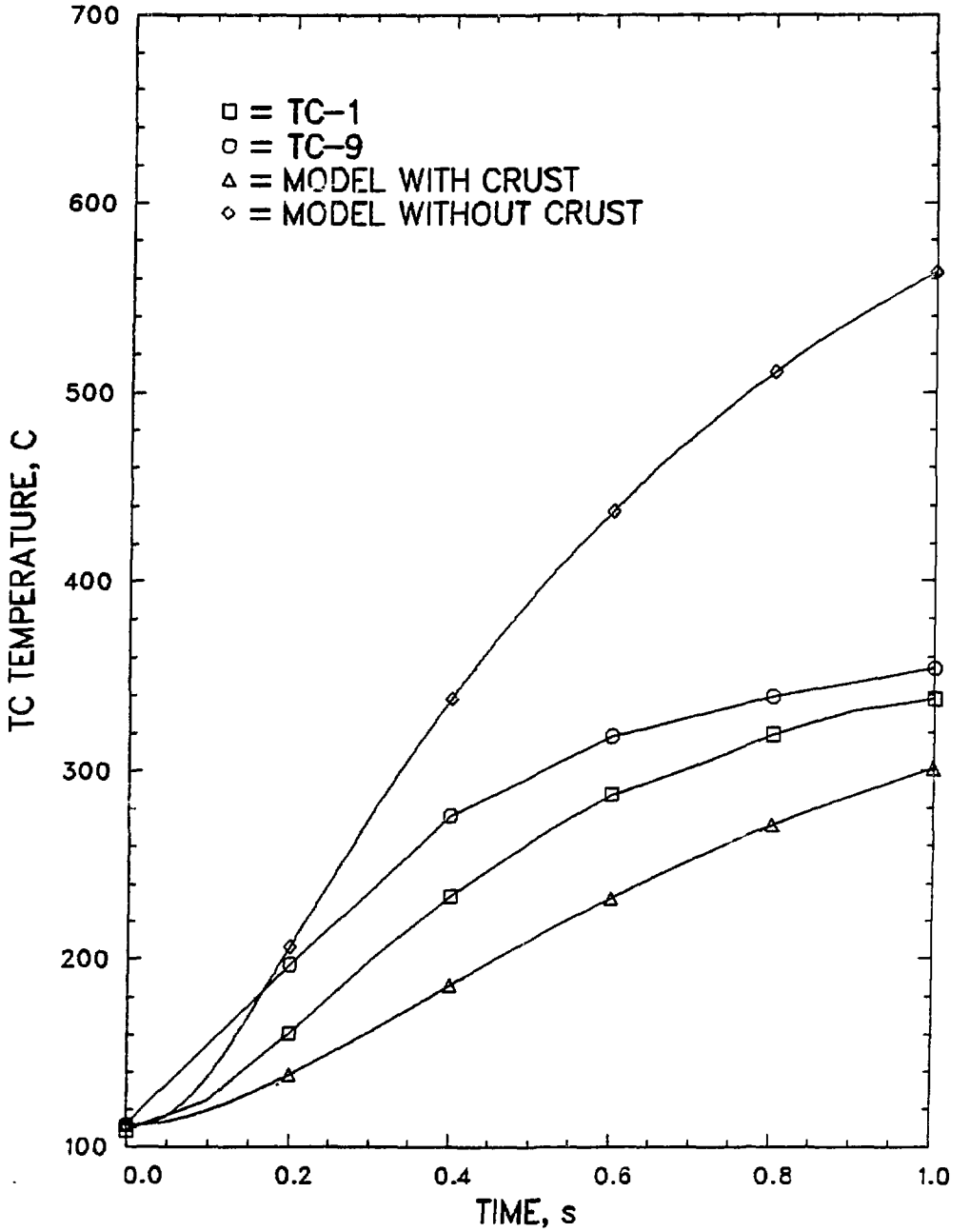

Figure 10. Comparison of Measured and Predicted Thermocouple Temperatures for CWTI-11: Thermocouples 2.54 cm from Centerline and 0.5 mm below Surface.

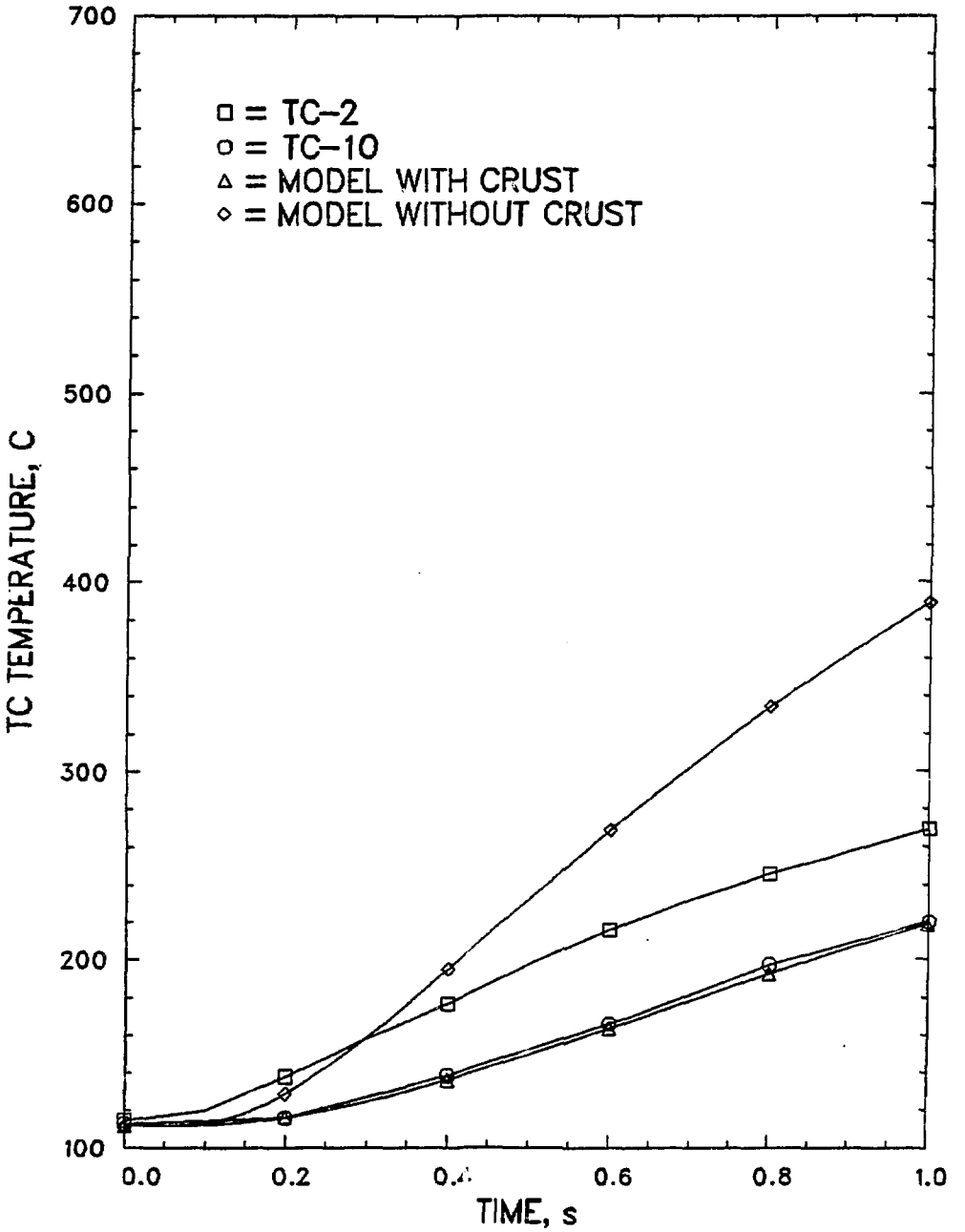

Figure 11. Comparison of Measured and Predicted Thermocouple Temperatures for CWTI-11: Thermocouples 2.54 cm from Centerline and 1.5 mm below Surface.

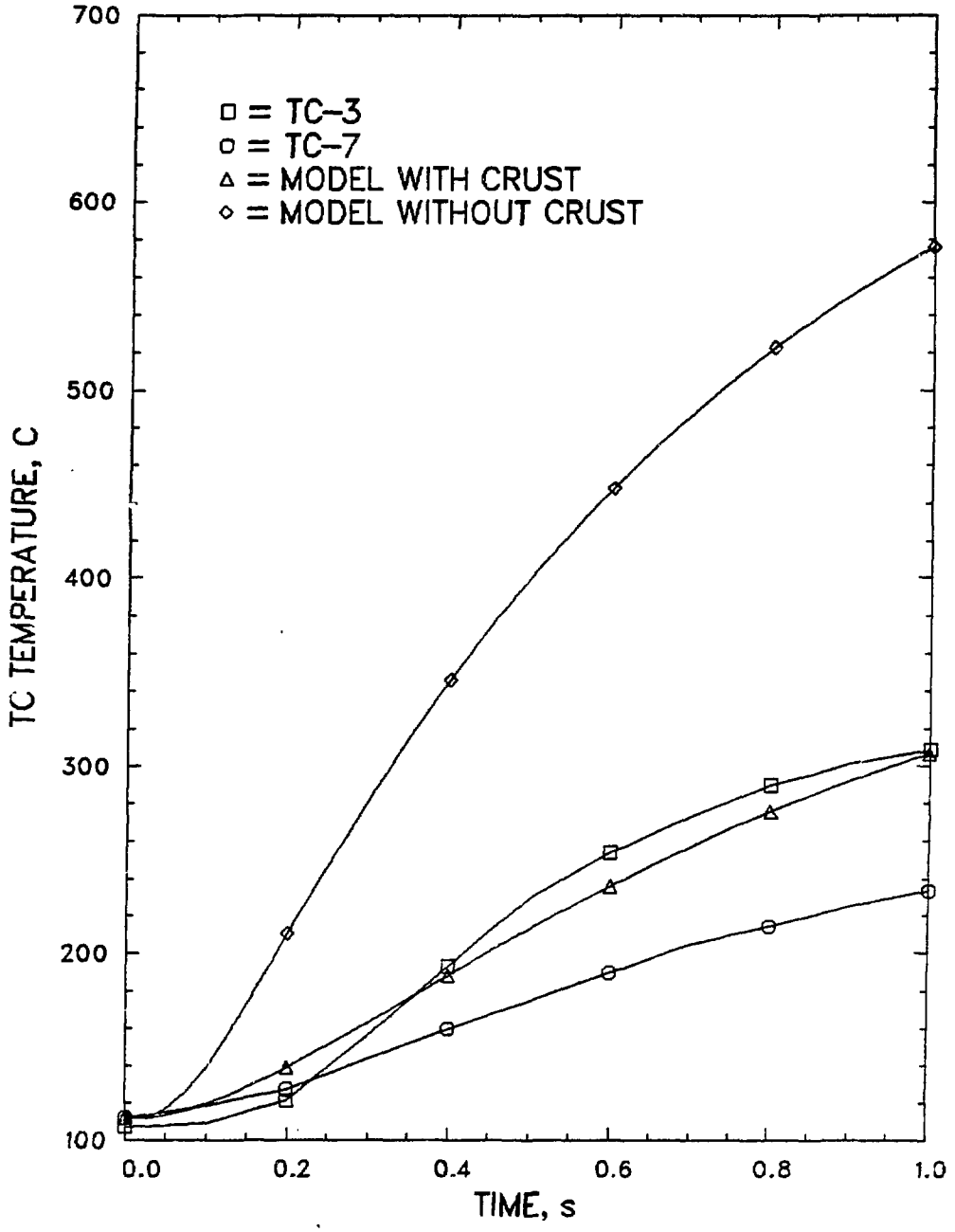

Figure 12. Comparison of Measured and Predicted Thermocouple Temperatures for CWTI-11: Thermocouples 1.27 cm from Centerline and 0.5 mm below Surface.

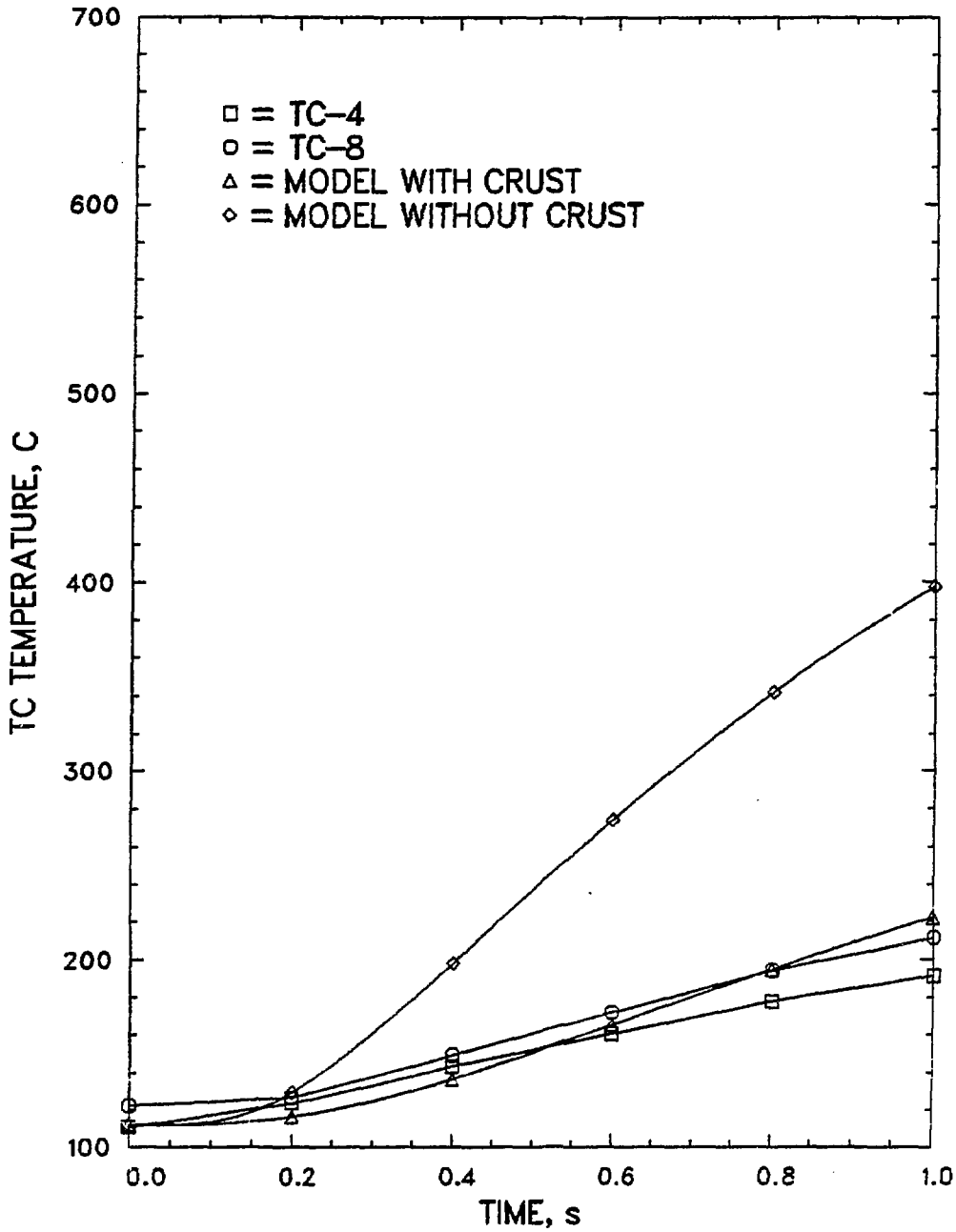

Figure 13. Comparison of Measured and Predicted Thermocouple Temperatures for CWTI-11: Thermocouples 1.27 cm from Centerline and 1.5 mm below Surface.

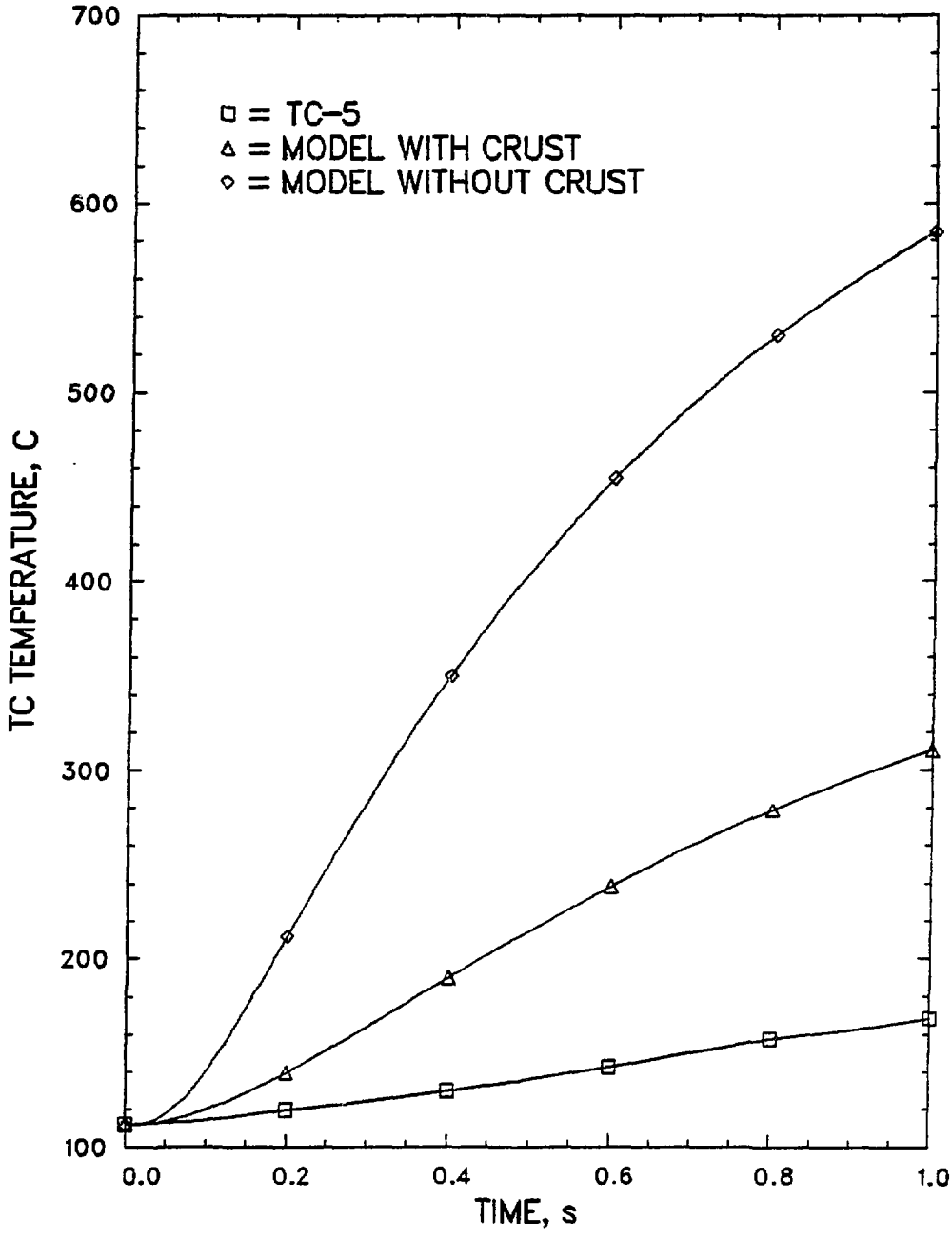

Figure 14. Comparison of Measured and Predicted Thermocouple Temperatures for CWTI-11: Thermocouples 0.24 cm from Centerline and 0.5 mm below Surface.

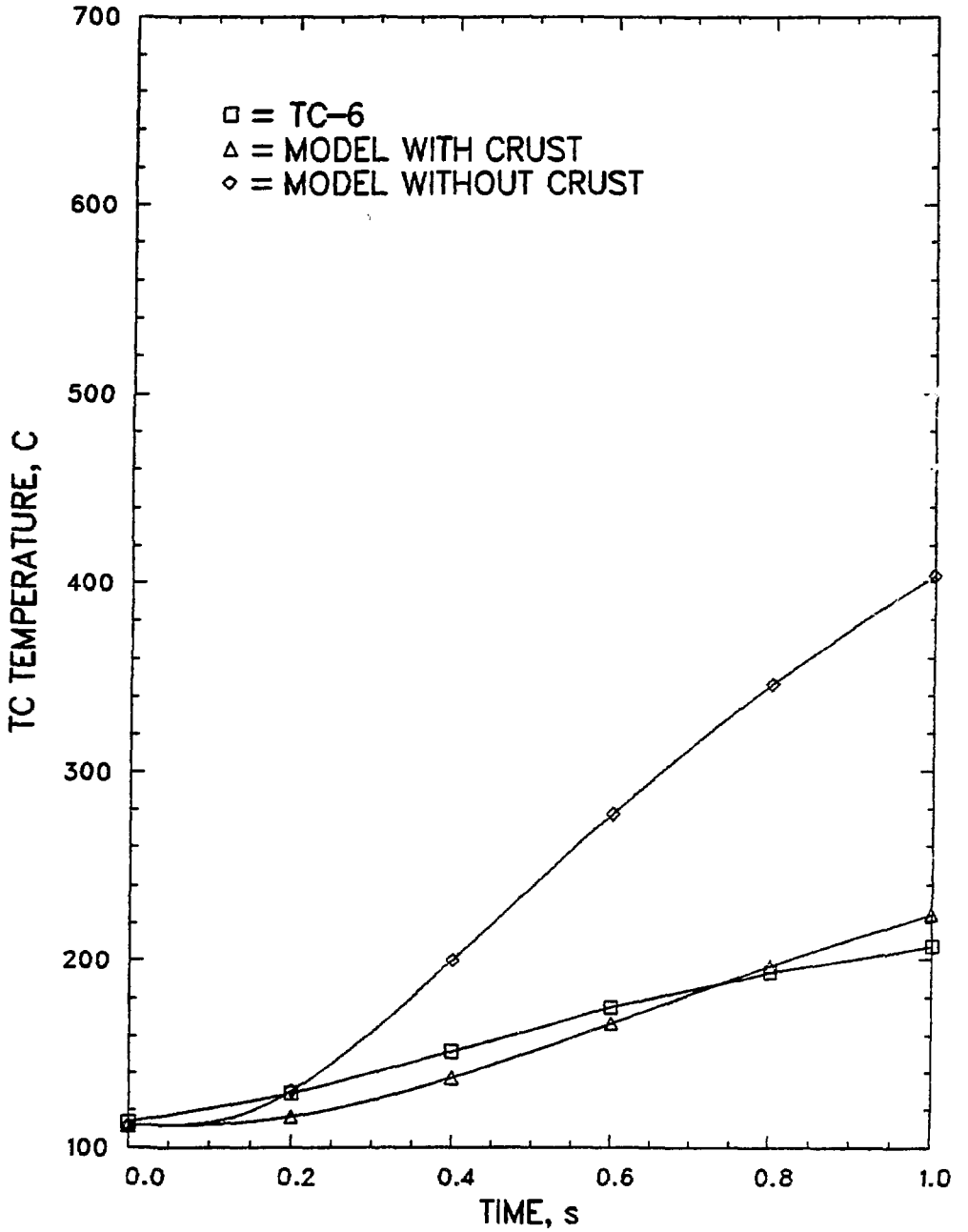

Figure 15. Comparison of Measured and Predicted Thermocouple Temperatures for CWTI-11: Thermocouples Located on Centerline and 1.5 *mm* below Surface.

NOTATION

D = jet diameter, m

h_{conv} = forced convection heat transfer coefficient, $W/(m^2 \cdot K)$

k = jet thermal conductivity, $W/(m \cdot K)$

L = heat of fusion, J/kg

$Nu = \frac{h_{conv} D}{k}$ = jet Nusselt number

Pr = jet Prandtl number

r = radial coordinate, m

Re = jet Reynolds number

T = temperature, K

t = time, s

z = axial/vertical coordinate, m

δ = crust thickness, m

ρ = density, kg/m^3

SUBSCRIPTS

f = corium "fuel"

$freeze$ = freezing temperature

i = corium/stainless steel interface

s = stainless steel

LITERATURE CITED

1. M. Epstein, M. J. Swedish, J. H. Linehan, G. A. Lambert, G. M. Hauser, and L. J. Stachyra, AIChE Journal, 26, p. 743 (1980).

2. B. W. Spencer, L. McUmber, J. J. Sienicki, R. Sehgal, and D. Squarer, "Results of Scoping Tests on Corium-Water Thermal Interactions in Ex-Vessel Geometry," Heat Transfer - Seattle 1983, ed. N. M. Farukhi, AIChE Symposium Series, No. 225, Vol. 79, p. 268, American Institute of Chemical Engineers, New York (1983).

3. B. W. Spencer, J. J. Sienicki, L. W. Deitrich, B. R. Sehgal, and D. Squarer, "Overview and Recent Results of ANL/EPRI Corium-Water Thermal Interaction Investigations," Proceedings International Meeting on Light Water Reactor Severe Accident Evaluation, Cambridge, MA, August 28-

September 1, 1983, Vol. 2, p. 15.2-1, American Nuclear Society, LaGrange Park (1983).

4. B. W. Spencer, L. M. McUmber, and J. J. Sienicki, "Results and Analysis of Reactor-Material Experiments on Ex-Vessel Corium Quench and Dispersal," Proceedings Fifth International Meeting on Thermal Nuclear Reactor Safety, Karlsruhe, Federal Republic of Germany, September 9-13, 1984.

5. H. Martin, "Heat and Mass Transfer between Impinging Gas Jets and Solid Surfaces," Advances in Heat Transfer, ed. J. P. Hartnett and T. F. Irvine, Jr., Vol. 13, p. 1, Academic Press, Inc., New York (1977).

6. V. N. Volkov and V. K. Li-Orlov, Heat Transfer-Soviet Research, 2, p. 41 (1970).

7. H. S. Carslaw and J. C. Jaeger, Conduction of Heat in Solids, Oxford at the Clarendon Press, Oxford (1959).